Editors' Suggestion | Featured in Physics

Pinning-Induced Folding-Unfolding Asymmetry in Adhesive Creases

Michiel A. J. van Limbeek,[1] Martin H. Essink,[2] Anupam Pandey,[3] Jacco H. Snoeijer,[2,*] and Stefan Karpitschka[1,†]

[1]*Max Planck Institute for Dynamics and Self-Organization, 37077 Göttingen, Germany*
[2]*Physics of Fluids Group, Mesa+ Institute, University of Twente, 7500 AE Enschede, Netherlands*
[3]*Biological and Environmental Engineering Department, Cornell University, Ithaca, New York 14853, USA*

(Received 24 March 2021; revised 11 June 2021; accepted 15 June 2021; published 9 July 2021; corrected 3 August 2021)

The compression of soft elastic matter and biological tissue can lead to creasing, an instability where a surface folds sharply into periodic self-contacts. Intriguingly, the unfolding of the surface upon releasing the strain is usually not perfect: small scars remain that serve as nuclei for creases during repeated compressions. Here we present creasing experiments with sticky polymer surfaces, using confocal microscopy, which resolve the contact line region where folding and unfolding occurs. It is found that surface tension induces a second fold, at the edge of the self-contact, which leads to a singular elastic stress and self-similar crease morphologies. However, these profiles exhibit an intrinsic folding-unfolding asymmetry that is caused by contact line pinning, in a way that resembles wetting of liquids on imperfect solids. Contact line pinning is therefore a key element of creasing: it inhibits complete unfolding and gives soft surfaces a folding memory.

DOI: 10.1103/PhysRevLett.127.028001

Creases are ubiquitous to nature and can readily be observed by closing ones' hand or bending ones' arm: Soft tissue responds to compression by folding into deep valleys of self-contacting skin [1–3]. The morphology of mammalian brains [4–7] or tumors [8] is dominated by creases that emerge from tissue growth under constraint conditions. Similarly, polymer coatings in technological applications may suffer from creasing due to swelling [9–13], but also compressed elastomers [1,14–16] and viscoelastic liquids [15] display this instability.

The canonical creasing behavior can be realized by uniaxially compressing a slab of a soft material [Fig. 1(a)]. Sharp creases form via a subcritical bifurcation after a reaching a critical strain ϵ_c [1,2]. When subsequently releasing the strain to below ϵ_c, the length of the crease is only gradually reduced. This implies bistability since either creased or homogeneous states can be found, depending on the deformation history [17–19]. Recent studies clarified the onset of creasing [2,20,21], invoking surface tension [17,18,22] or the presence of a skin [23] to explain the observed bistability.

Interestingly, a microscopic residual crease typically remains even after the strain is fully released to $\epsilon = 0$ [Fig. 1(a)]. This small feature, referred to as a "scar," is of great significance, since it serves as a nucleus for creases when repeating the compression [11,17,18]. As such, these scars endow soft materials with mechanical memory [11,17], offering a potential of dynamic programmability of surface folds. Despite their importance, scars have remained somewhat enigmatic. It was found that scars are not due to material failure, and their persistence was argued to originate from adhesion [16–18]. However, it is not clear whether adhesion and surface tension can actually lead to a reduction of surface energy compared to the flat, scarless state. Recent work focused on the consequences of surface tension to the onset bifurcation of creasing [22], but it is not known how surface tension affects folding and unfolding at the microscale.

In this Letter we resolve the micro- and macromorphology of adhesive creases by confocal microscopy [Fig. 1(b)], and identify the role of surface tension (γ), inside the self-contact. It is found that surface tension induces a second fold at the edge of the self contact, turning the surface into a T-shaped profile [Fig. 1(b), bottom right]. This involves a change of the contact angle θ from 180° for $\gamma \sim 0$ to 90° for $\gamma > 0$. Further, we show that folding and unfolding the crease are, at the microscale, intrinsically asymmetric processes. The unfolding is inhibited, and ultimately prevented, by contact line pinning. This pinning-induced hysteresis implies a new type of bistability, even far above the onset of creasing, and offers a natural explanation for the formation of scars.

Experimental.—A layer of a soft polymer gel (Dow Corning CY52-276, components A:B mixed 1:1 or 1.4:1

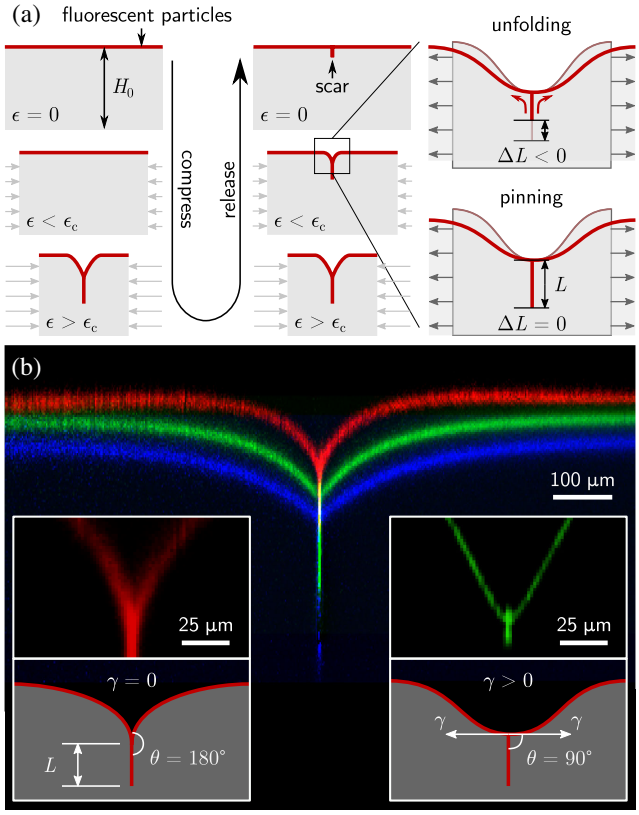

FIG. 1. (a) A uniaxially compressed soft material creases beyond a certain critical strain ϵ_c, folding its surface into a self-contact. The crease persists below ϵ_c, and scars remain even at $\epsilon = 0$: contact line pinning prevents complete unfolding. (b) Confocal images of creases for different elastocapillary lengths, $\ell = \gamma/G \approx 0$ (red), 20 (green), and 300 μm (blue). Insets: solid surface tension impacts the contact angle θ at the edge of the self-contact.

to obtain different shear moduli, thickness $H_0 \sim 1.0$ to 1.3 mm) was prepared on top of a stiff, uniaxially prestretched PVS rubber sheet (Zhermack Elite Double 20). To compress the gel layer, the prestretch of the support was slowly released by a micrometer [15,16]. Fluorescent particles (Invitrogen FluoSpheres, 100 nm diameter) were added to the bottom and top surface of the gel. Gel thickness and top surface morphology were measured with an upright confocal microscope (Leica TCS-SP2) with 10× and 40× magnification. To image the self-contact through the free surface with minimal optical artifacts, we used index-matched immersion liquids. The immersion also offers a way to tune the gel surface tension: We measured $\gamma \sim 0$ for the immersion with a long-chain silicone oil (Wacker, 12.5 Pa s) and $\gamma \sim 20$ mN/m for a water-glycerol mixture [16]. The relative importance of surface tension γ to shear modulus G is quantified by the elastocapillary length, $\ell = \gamma/G$. Importantly, these liquids caused virtually no swelling of the gel, as was tested by prolonged immersion. The typical compression protocol of an experiment is sketched in Fig. 1(a). First we increased the strain ϵ in small steps, recording after each step and a prolonged waiting time ($\gtrsim$15 min, much larger than the material relaxation time $\lesssim$0.5 s) the free-surface morphology by an xyz scan. After creases had formed we compressed a bit further, then repeated this procedure while decreasing ϵ again. Further experimental details can be found in the Supplemental Material [24].

Elastocapillary self-contact.—We first quantify the morphology of the elastocapilary self-contact, and how it is altered by surface tension. Figure 1(b) shows creased surface profiles from three experiments with different elastocapillary lengths: $\ell = \gamma/G \sim 0$ (red), ~20 μm (green, $G \sim 1.1$ kPa), and ~300 μm (blue, $G \sim 65$ Pa). Increasing the elastocapillary length amplifies the relative importance of surface tension, which on the macroscale leads to shallower indentations.

However, the most important consequence of $\gamma > 0$ is reflected in the micromorphology of the contact region (high magnification data, insets of Fig. 1(b). The angle θ that the surface describes at the contact line changes from a gentle touchdown with $\theta = 180°$ for $\gamma \sim 0$, to $\theta = 90°$ for $\gamma > 0$. Hence, besides the fold at the bottom of the crease, there is a second fold a the top of the self-contact where the surface profile acquires a T shape. On scales much smaller than ℓ, capillarity will be dominant over elasticity and we expect the contact angle to be given by Neumann's law [26–28]. In case of perfect self-adhesion, which is expected for soft polymer gels, the surface tension in the self-contact vanishes completely. The remaining balance of gel-liquid surface tensions implies the fold of $\theta = 90°$ [Fig. 1(b)], in good agreement with our experiments.

Consequential to this second fold is a strong curvature κ of the free surface near the contact line. When attempting to quantify this curvature, however, it turns out that κ does not reach a well-defined limiting value. Rather, it still grows as we reach our measurement resolution, which is well below the elastocapillary length. Figure 2 (purple markers) shows the measured curvature as a function of the distance to the contact line, for $\ell \sim 20$ μm. Surprisingly, the data suggest a logarithmic divergence of κ as the contact line is approached.

The logarithmic singularity of curvature is caused by the capillary boundary condition, which forces the material into a 90° angle. Analogous to the bottom of the crease [2,19,20], a fold of angle θ introduces a weak (logarithmic) stress singularity. For a neo-Hookean solid the stress singularity reads $p_{\mathrm{el}} = (\pi/\theta - \theta/\pi)G\ln(|x|) + p_0$ [29], where θ is the fold angle in radians and p_0 a gauge pressure. At the bottom of the self contact, where the crease was initiated, the fold has an angle $\theta = 2\pi$. In contrast, the two folds at the contact line involve an angle $\theta = \pi/2$, connecting the self-contact to the free surface in a T shape. Thus the elastic stress must be balanced by the Laplace pressure $\gamma\kappa = -p_{\mathrm{el}}$, which for a right angle gives the elastocapillary balance

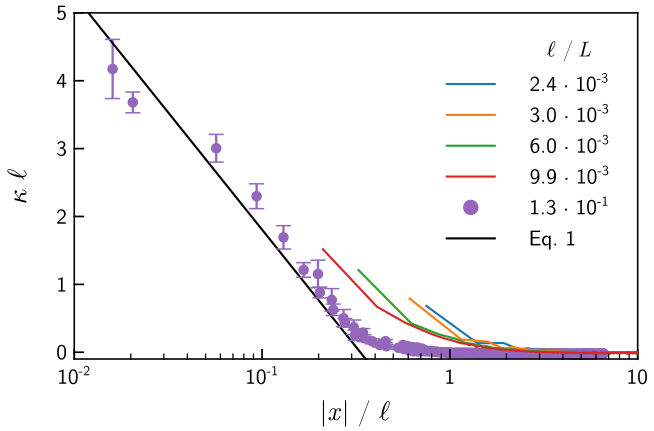

FIG. 2. Free surface curvature κ versus the horizontal distance x to the contact line, in units of the elastocapillary length $\ell = \gamma/G$. κ diverges logarithmically for $x \to 0$, both in experiments (symbols) and in simulations (lines). The horizontal shift between the curves reflects difference in gauge pressure p_0 in the log, which depends on the ratio ℓ/L. The experimental data was taken after compressing, for $\ell \sim 20\ \mu$m.

$$\gamma\kappa \simeq \frac{3}{2} G \ln\left(b\frac{\ell}{|x|}\right), \tag{1}$$

valid at distances $|x| \ll \ell$. Here we absorbed the gauge pressure p_0 into a dimensionless constant b. The prediction (1) is shown as the solid line in Fig. 2, in excellent agreement with the experimental data. We only adjusted the value of b, which cannot be derived by the local analysis of the singularity: it reflects a gauge pressure that is inherited from the full solution, invoking scales larger than ℓ.

To explore this effect, we performed finite element simulations of elastocapillary creases, assuming a neo-Hookean solid with constant surface tension (see Supplemental Material for details [24]). Numerical results are obtained for various ratios of ℓ/L, where L is the crease length. All numerical results exhibit the logarithmic divergence of curvature (Fig. 2, lines), following the prediction (1). The fact that the data are shifted laterally reflects the nonuniversality of b. Still, the numerical data gradually approach the experimental data as ℓ/L approaches the experimental value.

Thus we conclude that the capillary nature of adhesive creases has two important consequences at the microscale: (i) it governs the contact angle θ, implying a second fold at the top of the crease where the surface is T shaped. (ii) the fold, in turn, introduces a logarithmic singularity of the elastic stress and the surface curvature at the edge of the self-contact.

Intermediate asymptote.—Contrarily, for $x \gg \ell$, we expect capillary effects to play no role and hence, the problem should be described by a purely elastic solid mechanics. Then the crease length L becomes the relevant scale, and the morphology of the free surface was predicted to exhibit the scaling [19]

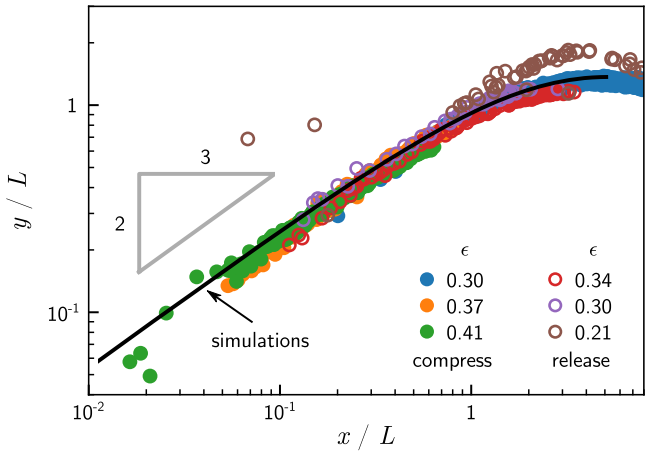

FIG. 3. Free surface profiles (experiment and simulation) for various ϵ for the case where $\gamma \approx 0$. The collapse of data confirms a universal shape that is governed by the crease length L, according to Eq. (2).

$$\frac{y - y_0}{L} \sim \left(\frac{x}{L}\right)^{2/3}, \tag{2}$$

where y_0 is the vertical coordinate of the contact line. This intermediate asymptote is expected to be valid whenever $\ell \ll x \lesssim L$. Figure 3 shows the collapse of simulations and measurements for $\gamma \sim 0$ and various ϵ, and confirms the $2/3$ exponent.

Folding-unfolding asymmetry.—Elastocapillary (inner) and elastic (intermediate) regions can be collapsed simultaneously by choosing the appropriate scales $x = l_x\hat{x}$ and $y = l_y\hat{y}$ on each axis. The inner, elastocapillary morphology (1), requires $l_x^2/l_y = \ell$ to collapse the data. The scaling behavior of the intermediate region (2), requires $l_y/l_x^{2/3} = L^{1/3}$. Both requirements are fulfilled simultaneously by choosing

$$l_x = \ell^{3/4}L^{1/4}, \qquad l_y = \ell^{1/2}L^{1/2}. \tag{3}$$

In Fig. 4, the original interface profiles (left panels) are shown next to the profiles as rescaled by the prediction (3) (right panels). The simulation data (top) almost collapse on a single curve, where the remaining difference can be attributed to the nonuniversal gauge pressure. The experimental data (bottom), by contrast, clusters into two groups. Filled symbols correspond to measurements after ϵ has been increased and form the upper master curve (folding). Open symbols correspond to measurements after ϵ has been decreased and form the lower master curve (unfolding).

The experiments show that the history of the crease is important for the observed morphology, even for $\epsilon > \epsilon_c$, where only the creased state is stable. The interface profiles

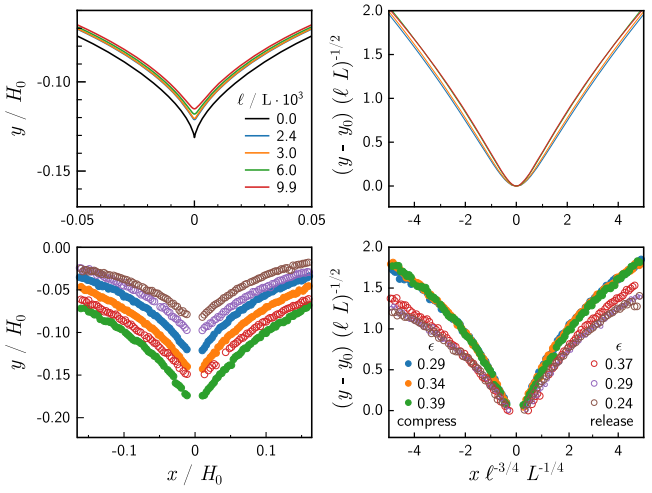

FIG. 4. Folding-unfolding asymmetry. Numerical (top) and experimental (bottom) profiles of the crease can be collapsed after rescaling by (3) (right panels). The experimental curves (elastocapillary length $\ell \sim 20$ μm) cluster into two sets, depending on whether the global compressive strain ϵ was increased (filled symbols) or decreased (open symbols) prior to the measurement. Surface profiles are shallower during unfolding than during folding.

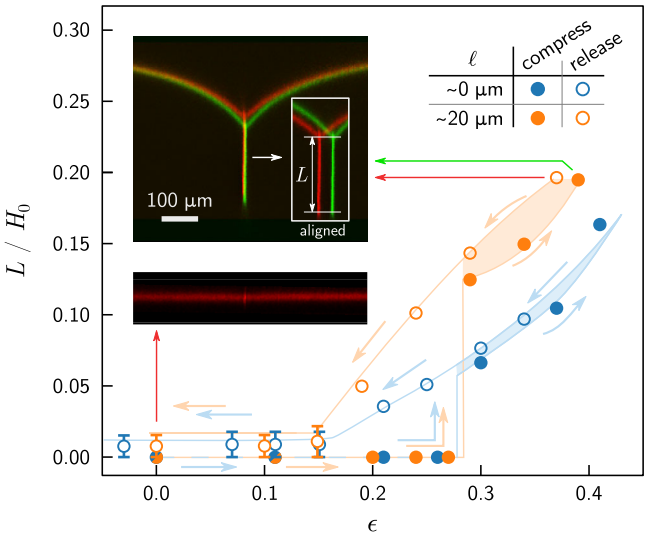

FIG. 5. Length of the self contact L as a function of global strain ϵ, for purely elastic ($\ell \sim 0$, blue) and adhesive, elastocapillary ($\ell \sim 20$ μm) creases. Two types of hysteresis can be observed: (i) the subcritical and critical transitions from the homogeneous to the creased state ($\epsilon \sim 0.28$), and back to homogeneous ($\epsilon \sim 0.15$), respectively. (ii) The creased state exhibits a manifold of possible L for each ϵ (shaded area). L depends on its history, reminiscent of contact line pinning. Upper inset: Two profiles of similar L but different ϵ (green: after a compression; red: after releasing). Lower inset: A tiny scar remains after full relaxation and even at $\epsilon < 0$. The error bars in the main plot reflect the uncertainty in determining the absolute size of the (residual) crease. As this merely provides a systematic offset to the length of developed creases, the uncertainty of the length hysteresis (shaded area) is much smaller (~0.005).

observed during folding are manifestly different from the profiles during unfolding, the latter being more shallow. This asymmetry between folding and unfolding is not observed in the simulations. For a given set of parameters, the numerical minimization of elastocapillary energy selects a unique crease morphology. Clearly, an element beyond equilibrium elastocapillary mechanics is required to properly interpret the experiments, which originates from contact line physics.

Contact line pinning.—The difference in morphologies upon switching from compression to expansion is visualized in the inset of Fig. 5. The green profile is taken during the compression phase, while the red profile is obtained after a subsequent release of strain. Clearly, the global indentation of the free surface decreased upon reducing ϵ, while the crease length L remained identical up to the measurement resolution. This offers direct evidence for contact line pinning, where there is no "unfolding" at all, i.e., no change of material points at the contact line [cf. sketch in Fig. 1(a)].

In the present context, the morphological hysteresis readily impacts the crease length L, which is no longer a pure function of the imposed strain ϵ. This is shown in Fig. 5 (main plot), reporting L versus ϵ. While bistability is well known below the onset of creasing, we here find an additional bistability that is caused by contact line pinning: the shaded area shows that, even well above the onset of creasing, the crease length still exhibits a history dependence. After increasing ϵ, smaller L are selected, rather than after decreasing ϵ, especially for $\ell \sim 20$ μm (orange curve, same data as in Fig. 4). For $\gamma \sim 0$, the measurement error is comparable to the detected hysteresis, and no definitive statement on its existence can be made. Because of experimental limitations we can only give an upper bound for the scar length ~10 μm. However, the fact that this hysteresis loop becomes more pronounced for larger ℓ suggests a capillary origin of contact line pinning.

The observed contact line pinning is analogous to the wetting of liquids on solid surfaces [30]. In that case, the motion of solid-liquid-vapor three-phase contact lines is arrested by pinning on heterogeneities of the solid surface. Such heterogeneities lead to a complicated energy landscape which allows for a range of stable liquid morphologies, leading to a range of contact angles. The pinning observed for creasing could be of similar origin as in wetting, where an energetic barrier $\Delta\gamma$ is required to move the contact line across features of the surface topography. We therefore expect a range of mechanically stable crease lengths of the order of $\Delta L \sim \Delta\gamma/G$. This ultimately prevents complete unfolding: the remaining elastic energy is not sufficient to overcome this pinning barrier. This explanation for scars is similar to that given in Ref. [18], which was phrased in terms of an energy release rate rather than $\Delta\gamma$. From our findings, however, it is clear that the

energy release rate for unfolding an adhesive crease cannot be given by the reversible work of self-adhesion, based on surface energies, as that would not offer a mechanism for contact line pinning. Indeed, our finite element simulations (with reversible adhesion) do not give a folding-unfolding asymmetry. They lack the new bistability indicated by the shaded areas in Fig. 5, and do not admit any scars. To exclude the tracer particles as cause for the scars in our experiments, we also tested an uncoated specimen by brightfield reflection microscopy, finding the same behavior (see Supplemental Material [24]). Our explanation in terms of contact line pinning is also consistent with the observation of scar annealing on long timescales [16,18]: once again, this resembles the case of liquid wetting, where contact line pinning can indeed be overcome by thermal activation [31–33].

Outlook.—Our confocal microscopy experiments have revealed an intrinsic folding-unfolding asymmetry, induced by contact line pinning, that offers a natural explanation for scars. Pinning is therefore a central element in creasing that needs to be accounted for in theory and simulations, and offers a way to articulate the role of "defects." In addition, we have shown that surface tension dictates the mechanics at scales below the elastocapillary length, folding the solid into well-defined contact angles. As such, the crease morphology opens a new route to quantify solid-solid interfacial mechanics, in line with recent developments for solid-liquid interfaces [27,34]. Understanding the interfacial micromechanics of soft materials unfolds their potential as programmable matter [35], impacting, for instance, soft robotics [36], biomolecular patterning [12], or smart textiles [37].

S. K. acknowledges funding from the German research foundation (DFG, Project No. KA4747/2-1), and M. H. E. and J. H. S. from NWO through VICI Grant No. 680-47-632.

*j.h.snoeijer@utwente.nl
†stefan.karpitschka@ds.mpg.de

[1] A. N. Gent and I. S. Cho, Surface instabilities in compressed or bent rubber blocks, Rubber Chem. Technol. **72**, 253 (1999).
[2] W. Hong, X. Zhao, and Z. Suo, Formation of creases on the surfaces of elastomers and gels, Appl. Phys. Lett. **95**, 111901 (2009).
[3] J. Dervaux and M. Ben Amar, Mechanical instabilities of gels, Annu. Rev. Condens. Matter Phys. **3**, 311 (2012).
[4] T. Tallinen, J. Y. Chung, J. S. Biggins, and L. Mahadevan, Gyrification from constrained cortical expansion, Proc. Natl. Acad. Sci. U.S.A. **111**, 12667 (2014).
[5] B. Mota and S. Herculano-Houzel, Cortical folding scales universally with surface area and thickness, not number of neurons, Science **349**, 74 (2015).
[6] T. Tallinen, J. Y. Chung, F. Rousseau, N. Girard, J. Lefèvre, and L. Mahadevan, On the growth and form of cortical convolutions, Nat. Phys. **12**, 588 (2016).
[7] E. Karzbrun, A. Kshirsagar, S. R. Cohen, J. H. Hanna, and O. Reiner, Human brain organoids on a chip reveal the physics of folding, Nat. Phys. **14**, 515 (2018).
[8] J. Dervaux, Y. Couder, M.-A. Guedeau-Boudeville, and M. Ben Amar, Shape Transition in Artificial Tumors: From Smooth Buckles to Singular Creases, Phys. Rev. Lett. **107**, 018103 (2011).
[9] A. Onuki, Theory of pattern formation in gels: Surface folding in highly compressible elastic bodies, Phys. Rev. A **39**, 5932 (1989).
[10] H. Tanaka and T. Sigehuzi, Surface-pattern evolution in a swelling gel under a geometrical constraint: Direct observation of fold structure and its coarsening dynamics, Phys. Rev. E **49**, R39 (1994).
[11] V. Trujillo, J. Kim, and R. C. Hayward, Creasing instability of surface-attached hydrogels, Soft Matter **4**, 564 (2008).
[12] J. Kim, J. Yoon, and R. C. Hayward, Dynamic display of biomolecular patterns through an elastic creasing instability of stimuli-responsive hydrogels, Nat. Mater. **9**, 159 (2010).
[13] M. Ben Amar and P. Ciarletta, Swelling instability of surface-attached gels as a model of soft tissue growth under geometric constraints, J. Mech. Phys. Solids **58**, 935 (2010).
[14] A. Ghatak and A. L. Das, Kink Instability of a Highly Deformable Elastic Cylinder, Phys. Rev. Lett. **99**, 076101 (2007).
[15] S. Mora, M. Abkarian, H. Tabuteau, and Y. Pomeau, Surface instability of soft solids under strain, Soft Matter **7**, 10612 (2011).
[16] S. Cai, D. Chen, Z. Suo, and R. C. Hayward, Creasing instability of elastomer films, Soft Matter **8**, 1301 (2012).
[17] J. Yoon, J. Kim, and R. C. Hayward, Nucleation, growth, and hysteresis of surface creases on swelled polymer gels, Soft Matter **6**, 5807 (2010).
[18] D. Chen, S. Cai, Z. Suo, and R. C. Hayward, Surface Energy as a Barrier to Creasing of Elastomer Films: An Elastic Analogy to Classical Nucleation, Phys. Rev. Lett. **109**, 038001 (2012).
[19] S. Karpitschka, J. Eggers, A. Pandey, and J. H. Snoeijer, Cusp-Shaped Elastic Creases and Furrows, Phys. Rev. Lett. **119**, 198001 (2017).
[20] P. Ciarletta, Matched asymptotic solution for crease nucleation in soft solids, Nat. Commun. **9**, 496 (2018).
[21] P. Ciarletta and L. Truskinovsky, Soft Nucleation of an Elastic Crease, Phys. Rev. Lett. **122**, 248001 (2019).
[22] Q. Liu, T. Ouchi, L. Jin, R. Hayward, and Z. Suo, Elastocapillary Crease, Phys. Rev. Lett. **122**, 098003 (2019).
[23] E. Hohlfeld and L. Mahadevan, Unfolding the Sulcus, Phys. Rev. Lett. **106**, 105702 (2011).
[24] See Supplemental Material at http://link.aps.org/supplemental/10.1103/PhysRevLett.127.028001 for additional details about the experiments and the simulations, which includes Ref. [25].
[25] M. Heil and A. Hazel, oomph-lib: An object-oriented multiphysics finite-elementlibrary, in *Fluid-Structure Interaction*, edited by M. Schäfer and H.-J. Bungartz (Springer, New York, 2006), pp. 19–49.

[26] S. Karpitschka, L. van Wijngaarden, and J. H. Snoeijer, Surface tension regularizes the crack singularity of adhesion, Soft Matter **12**, 4463 (2016).
[27] Q. Xu, K. E. Jensen, R. Boltyanskiy, R. Sarfati, R. W. Style, and E. R. Dufresne, Direct measurement of strain-dependent solid surface stress, Nat. Commun. **8**, 1 (2017).
[28] A. Pandey, B. Andreotti, S. Karpitschka, G. J. van Zwieten, E. H. van Brummelen, and J. H. Snoeijer, Singular Nature of the Elastocapillary Ridge, Phys. Rev. X **10**, 031067 (2020).
[29] M. Singh and A. C. Pipkin, Note on Ericksen's problem, Z. Angew Math. Phys. **16**, 706 (1965).
[30] D. Bonn, J. Eggers, J. Indekeu, J. Meunier, and E. Rolley, Wetting and spreading, Rev. Mod. Phys. **81**, 739 (2009).
[31] E. Rolley and C. Guthmann, Dynamics and Hysteresis of the Contact Line between Liquid Hydrogen and Cesium Substrates, Phys. Rev. Lett. **98**, 166105 (2007).
[32] J. H. Snoeijer and B. Andreotti, Moving contact lines: Scales, regimes, and dynamical transitions, Annu. Rev. Fluid Mech. **45**, 269 (2013).
[33] H. Perrin, R. Lhermerout, K. Davitt, E. Rolley, and B. Andreotti, Defects at the Nanoscale Impact Contact Line Motion at all Scales, Phys. Rev. Lett. **116**, 184502 (2016).
[34] B. Andreotti and J. H. Snoeijer, Statics and dynamics of soft wetting, Annu. Rev. Fluid Mech. **52**, 285 (2020).
[35] E. Hawkes, B. An, N. M. Benbernou, H. Tanaka, S. Kim, E. D. Demaine, D. Rus, and R. J. Wood, Programmable matter by folding, Proc. Natl. Acad. Sci. U.S.A. **107**, 12441 (2010).
[36] D. Rus and M. T. Tolley, Design, fabrication and control of soft robots, Nature (London) **521**, 467 (2015).
[37] N.-K. Persson, J. G. Martinez, Y. Zhong, A. Maziz, and E. W. H. Jager, Actuating textiles: Next generation of smart textiles, Adv. Mater. Technol. **3**, 1700397 (2018).

Correction: The omission of a marker indicating "Featured in Physics" has been fixed.